

## Analysis of Crashback Forces Compared with Experimental Results

Scott Black and Susan Swithenbank

Naval Surface Warfare Center, Carderock Division, Bethesda MD, U.S.A.

### ABSTRACT

Crashback occurs when a ship is moving forward, but the propeller is operating in reverse. This condition happens when a ship is trying to stop as quickly as possible. Propellers can experience structural failures during high power crashback maneuvers.

This analysis examines the velocities measured during a crashback experiment on a model propeller using particle-image velocimetry. The propeller was tested both as an open propeller and with the propeller operating inside of a duct. The data was analyzed to look at the velocities in the mean and extreme loading conditions for a range of crashback advance coefficients. These mean and extreme loading conditions were then used in a strip theory approach to develop loads for finite element analysis that examined stresses on the individual blades. These stresses were compared with experimental strain measurements.

### Keywords

Propeller, crashback, FEA, PIV, experiments

### 1 INTRODUCTION

The crashback condition is one of the most complex and challenging propeller operating conditions to analyze. The propeller loading during crashback has a steady time-average component, but is dominated by large unsteady hydrodynamic forces. Some of the unsteady forces are broadband in nature, while a portion of the forces are at low frequency and can contribute to propeller maneuvering forces. The low frequency unsteadiness also results in the most extreme propeller blade loading conditions.

Prior to a crashback maneuver, the initial advance coefficient is typically around +1. As the crashback transient begins, the propeller is quickly brought to a stop, during which time the advance coefficient,  $J$ , increases from a value of +1 to infinity, or in the ITTC nomenclature, an advance angle,  $\beta^*$ , of  $24^\circ$  to  $90^\circ$ . As the propeller RPM begins to reverse, the propeller enters the crashback, or second-quadrant, of the open water chart with an advance coefficient of negative infinity and begins to move towards zero as the ship continues to slow and the negative RPM increases to some motor or shafting defined limit ( $\beta^* = 90^\circ$  towards  $180^\circ$ ). A sample full scale time history of advance coefficient is shown in Figure 1. If the advance coefficient actually reached zero, the vessel would be at a complete stop.

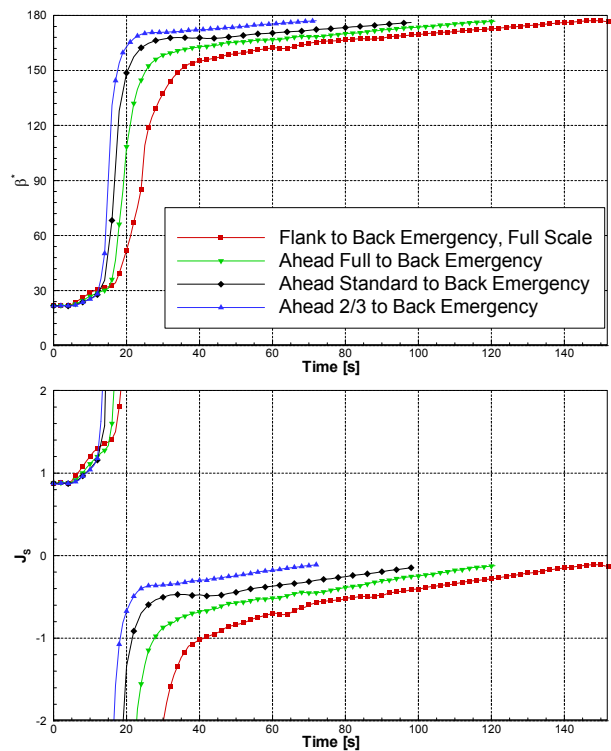


Figure 1. Example full scale trial data showing the change in advance coefficient and angle over time.

Since most prime movers and shafting have torque limits, the largest reverse power typically is not applied until the shafting achieves its full astern RPM. Based on full scale trial data for several vessels, typical ships will have slowed down significantly by the time the maximum negative RPM is achieved and by that time, the advance coefficient is in the range of -1 to -0.5, where potential flow codes may be able to predict realistic loads of the mean hydrodynamic loadings.

Unfortunately, the mean crashback loading is not a sufficient analysis condition to evaluate a propeller design structurally. Strain gage measurements have determined at both model and full scale that the extreme strain at the root can be as much as 2.5 times higher than the mean root strain [Jessup et al. (2006)].

The crashback condition is dominated by the interaction of the free stream flow field with strong recirculation driven by the local propeller-induced velocity. The local

propeller-induced velocity pushes the fluid against the incoming free stream flow. The fluid then passes around the outside of the propulsor where it is then pulled back into the unit. The vortex ring created in this condition is unsteady even in the idealized conditions of a water tunnel. Extreme flow unsteadiness and the varying degrees of blade surface flow separation make prediction of individual blade forces challenging even with large eddy simulations [Chang et al. 2008].

This study analyzed velocity measurements of an open and ducted propeller using a blade element approach to determine which inflow conditions cause the most extreme loadings to the blades. These inflows were used to develop pressure loads that were imposed on a finite element model of the blade. The resulting structural analysis results are compared to experimental strain gage measurements.

## 2 TEST DESCRIPTION

The Particle Image Velocimetry (PIV) data experiments were conducted in the 36-inch variable pressure water tunnel (VPWT) at the Naval Surface Warfare Center in Carderock, MD (NSWCCD). The PIV data was acquired in the vertical transverse plane. The experimental setup is shown in Figure 2. The propeller model used in the experiment was model number 4381, a five-bladed, twelve-inch diameter propeller with no skew or rake [Hecker and Remmers (1971)]. The data analyzed in this report was taken in September and October of 2004 and June of 2005. The data acquired in 2004 was in the open configuration. In 2005 data was acquired in both the open and ducted configurations. In the ducted configuration, non-lifting stators upstream of the propeller supported the duct.

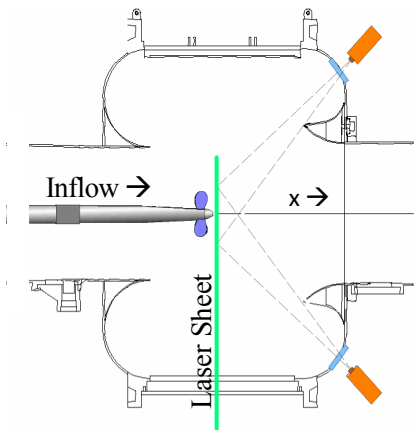


**Figure 2. PIV set-up in the 36" water tunnel for Y-Z measurement planes.**

During normal ahead operations, the PIV plane was slightly downstream of the propeller. The propeller plane is at the center of the 2.5 inch long hub. For the open configuration the PIV data was acquired at 2.44 inches from the propeller plane. For the ducted configuration, the edge of the duct was 3.89 inches from the propeller

plane, which was 0.5 inches downstream of the trailing edge of the duct. Advance coefficient values of to -0.3, -0.5, -0.7 and -1.0 were investigated. For more information on the experimental set-up, refer to Jessup et al. (2006, 2007).

For each advance coefficient, 1024 PIV images were acquired at 35 Hz. These images were measured at four advanced coefficients for the open and ducted configurations. The images were collected in three of four series that were separated by several minutes. The rotor RPM was 700 for all conditions.

An additional test conducted in 2008 used the same set-up as the original PIV experiment, though PIV data was not taken. Instead, a strain gauge mounted at 35% radius was used to find the principle strain in the blade [Swithenbank et al. (2008)].

## 3 PIV ANALYSIS

The goal of the PIV analysis is to estimate the mean and unsteady propeller blade thrust and root bending moment in the crashback condition using the measured velocities. The analysis produces spanwise distributions of the axial and tangential velocities, angle of attack, and root bending moments for the average and most extreme crashback loading conditions.

The same PIV total velocity data has been used previously as inputs to an unsteady lifting surface analysis to compute side forces with limited success [Jessup et al. (2006)].

The PIV data was acquired in X-Y-Z coordinates. For this analysis and comparison to previous results, cylindrical coordinates were used. The advanced angle,  $\beta$ , is the inverse tangent of the ratio of the axial and tangential velocities relative to the moving blade.  $\beta$  in radians is defined as:

$$\beta(r) = \tan^{-1}\left(\frac{U_x}{\omega r + U_t}\right) \quad (1)$$

where  $U_x$  is the velocity in the x-direction at a given location,  $U_t$  is the velocity in the  $\theta$ -direction,  $\omega$  is the rotational speed on the propeller in radians per second, and  $r$  is the radius. Figure 3 is a diagram illustrating the advanced angle,  $\beta$ , with respect to the propeller for both the ahead and crashback conditions.

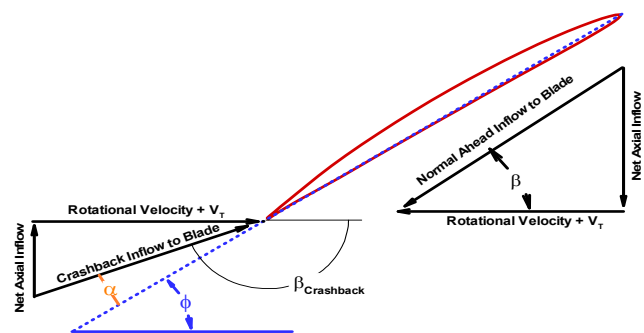


**Figure 3. Diagram showing the beta angle.**

The two-dimensional angle of attack,  $\alpha$ , in the ahead inflow condition is computed as the difference between the local pitch and the inflow angle. The approximation for the lift coefficient is derived from the two-dimensional flat plate lift-slope curve. The lift coefficient,  $C_{L-2D}$ , is defined as:

$$C_{L-2D}(r) = 2\pi\alpha(r) \quad (2)$$

The lift from a segment of propeller blade is less than that from a two-dimensional analysis. To correct for this, a correlation factor, which is particular to the blade geometry needs to be developed. For this analysis, the correction factor was determined from steady backing analysis using a lifting surface analysis code at two advance coefficients to define:

$$F(r) = C_{L-3D}(r) / C_{L-2D}(r) \quad (3)$$

For the geometry studied here, the average value of  $F$  was approximately 0.18. For this analysis, the axial and tangential velocities were averaged over the projected chord at each radius to compute an average inflow angle. That inflow angle was used to compute the local angle of attack,  $\alpha$ , and the lift. The average lift over the chord,  $L$ , at each radius is defined as:

$$L(r) = \frac{1}{2} \rho * C_{L-3D}(r) * U_{tot}^2 * c(r) \quad (4)$$

where  $c(r)$  is the local chord,  $\rho$  is the fluid density and  $U_{tot}$  is the total velocity including, the axial component, the tangential component and the speed of the propeller such that  $U_{tot}$  is:

$$U_{tot} = \sqrt{U_x^2(r) + (\omega r + U_g(r))^2} \quad (5)$$

The average thrust per unit chord as a function of radius is:

$$T(r) = L(r) * \cos(\beta(r)) \quad (6)$$

The total thrust for a single blade is the integral over the entire blade:

$$T_{tot} = \int_{r_{hub}}^R T(r) dr \quad (7)$$

The bending moment relative to the root blade section from a single radius is:

$$M_R(r) = L(r) * (r - r_{hub}) * \cos(\beta(r) - \phi(r_{hub})) \quad (7)$$

where  $r_{hub}$  is the radius of the hub and  $\phi$  is the local blade pitch. The total bending moment at the root is the integral of all the bending moments over the entire blade.

$$M = \int_{r_{hub}}^R M_R(r) dr \quad (8)$$

In this analysis thirty radii were used between the hub and the tip of the propeller. Integrations with increased resolution were not found to change the results significantly. An sample projection of the 4381 propeller on the average axial velocity at  $J=-0.7$  is shown in Figure 4.

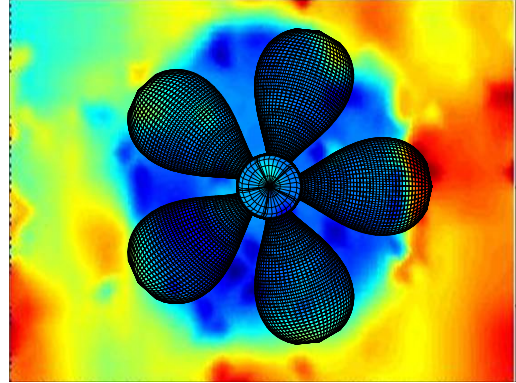


**Figure 4. Propeller 4381 superimposed on the average axial PIV data at  $J=-0.7$ .**

#### 4 HYDRODYNAMIC PREDICTIONS

In the crashback quadrant, the propeller is operating at a positive ship speed,  $V_s$ , and a negative RPM, resulting in a negative advance coefficient ( $J$ ). Both the thrust and torque on the propeller are negative during crashback. In the advance coefficient range of 0 to -0.5, the propeller blades are operating in what is similar to a steady backing operating condition. The induced velocities from the propeller are sufficiently strong to fully reverse the flow through the propeller disk, and the blade sections operate with attached flows. For lower values of advance coefficient, the angles of attack of the blade sections increase, resulting in stalled performance that rapidly increases the negative non-dimensional thrust and torque.

Potential flow analysis codes are commonly used for the analysis of marine propellers, however they require certain assumptions regarding well behaved attached flow and thin boundary layers. For propeller 4381 in crashback advance coefficients below -0.5, the presence of flow separation and complex shed wakes make the predictions from these types of tools inaccurate.

The black symbols in Figure 5 show the predictions generated using the potential flow panel method code PSF-10 for the ahead and backing quadrants [Kerwin and Lee (1978)]. The backing quadrant predictions were performed by reversing the blade geometry such that the leading edge becomes the trailing edge while the sign of the rake, skew and camber are reversed. Additionally, the thickness at what is normally the leading edge was modified to create a wedge shape since the panel method's iterative pressure Kutta condition has trouble converging in the case of a blunt trailing edge. The potential flow code shows good agreement with the towing tank performance data in the ahead and backing quadrants.

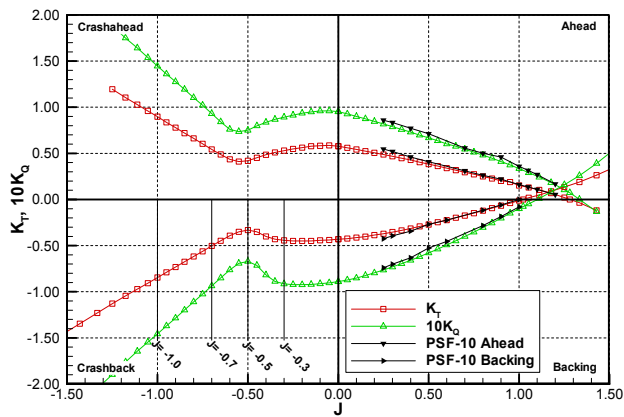


**Figure 5. Thrust and torque predictions for open propeller 4381.**

There is not yet an agreed upon approach for computing the hydrodynamic loading during crashback that captures the unsteady, extreme loading events that are believed to produce structural failures. The Large Eddy Simulation work being pursued by Vysohlid and Mahesh (2006) has shown great promise for predicting crashback flows, but is expected to remain a time-consuming calculation that will be difficult to exercise for routine designs for several more years.

In order to study the structural loads during crashback, in 2000-2001 a process for predicting hydrodynamic loading during crashback was developed at the Naval Surface Warfare Center, Carderock Division (NSWCCD). In 2001, a rough order of magnitude (ROM) procedure was developed to calculate hydrodynamic loads based on X-R plane PIV data from a test on a propeller operating in crashback in the 36" VPWT. The ROM method is composed of a mean and worst case loading analysis procedure. The mean crashback loading is based on a steady backing analysis using a potential flow analysis code in the measured circumferential mean inflow. The extreme loading is based on the PIV measured variations in inflow. The extreme 3-D loading is based on the 2-D angle-of-attack change between the average and a worst-case velocity. The 2-D to 3-D angle of attack corrections are based on lifting surface analysis. A flat plate loading is superimposed on the mean loading as a classic flat-plate angle of attack pressure jump. The worst-case PIV velocity was determined by looking at just the change in axial velocity over the span since no tangential velocity was then available.

This procedure has subsequently been updated based on strain gauge measurements and PIV data in the X-Y plane obtained on the 4381 propeller in 2004 [Jessup et al. 2004]. This process is continually being improved with further analysis and experimental data.

The mean crashback analysis is performed using a panel method analysis tool where the analysis assumes a quasi-steady backing condition.

## 5 MEAN CRASHBACK ANALYSIS

For each advance coefficient, the circumferential mean of the axial velocity, tangential velocity,  $\alpha$ ,  $\beta$ , thrust and the bending moment versus radius were calculated. Figure 6 shows the circumferential mean axial velocities for all the J values in both the open and ducted configurations. For the open configuration the axial velocities are similar in magnitude to the tunnel speed,  $U_s$ , though opposite in direction. For the ducted configuration the axial velocity is up to 2.5 times the magnitude of the tunnel velocity at a J of -0.3, but at the J values of -0.7 and -1.0 the velocity is similar to the open configuration.

The circumferential mean tangential velocities are shown in Figure 7 for both the open and ducted configurations. The stators in the ducted configuration greatly reduced the tangential velocities for all cases except a J of -1.0 where an increase is seen at the outer radius. The tangential velocities are on average one-tenth the magnitude of the axial velocities.

The contribution of the lift from each chord-wise strip to the root bending moment was computed using the circumferential-mean, time-averaged velocities. The bending moment was calculated as the mean in time for each chord-wise strip across the span of the blade. The bending moment contributions versus radius are shown in Figure 8 for the open and ducted configurations. The open and ducted configurations show similar magnitudes for the bending moment at the root, though the J values differ for the largest bending moment between the open and ducted configurations.

The open water predictions for open propeller 4381 in the crashback quadrant are shown in Figure 9 from both water tunnel and open water towing tank measurements. These calculations utilized the PIV measured velocities at a downstream plane to determine the time averaged total inflow into the propeller. The panel-method potential flow software PSF-10 [Kerwin and Lee (1978)] was used with a field point velocity program SFPV, to iteratively determine the effective inflow by subtracting the propeller induced velocities from the measured total velocity.

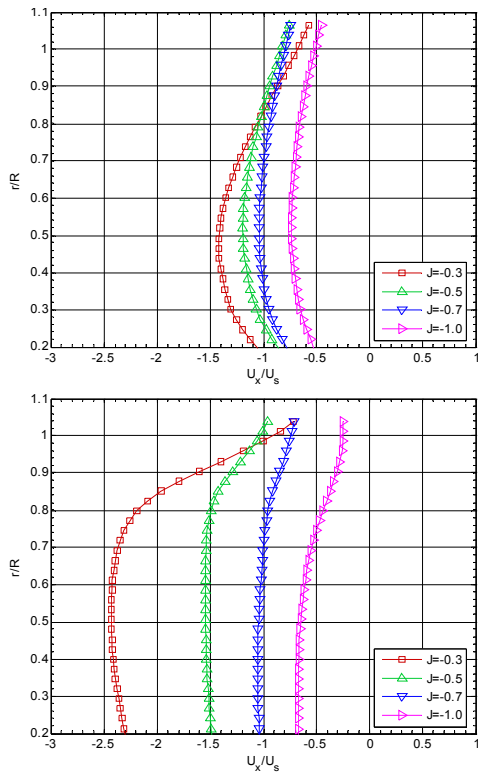


Figure 6. The circumferential mean axial velocities versus radius for the open configuration (top) and the ducted configuration (bottom).

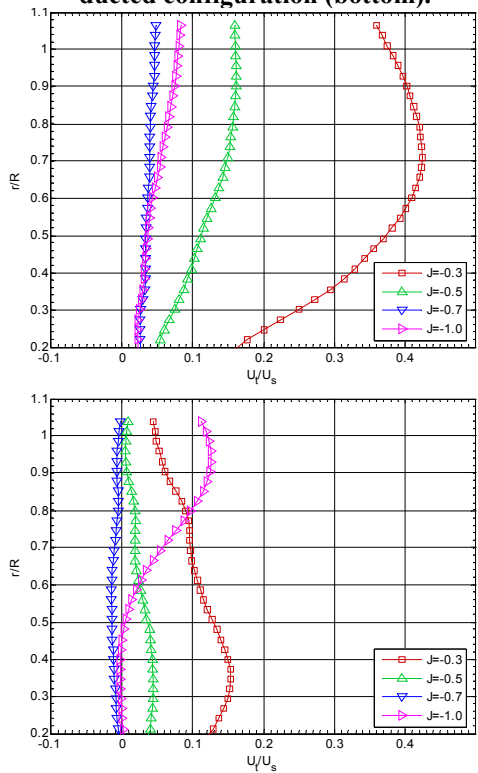


Figure 7. The circumferential mean tangential velocities for versus radius for the open configuration (top) and the ducted configuration (bottom).

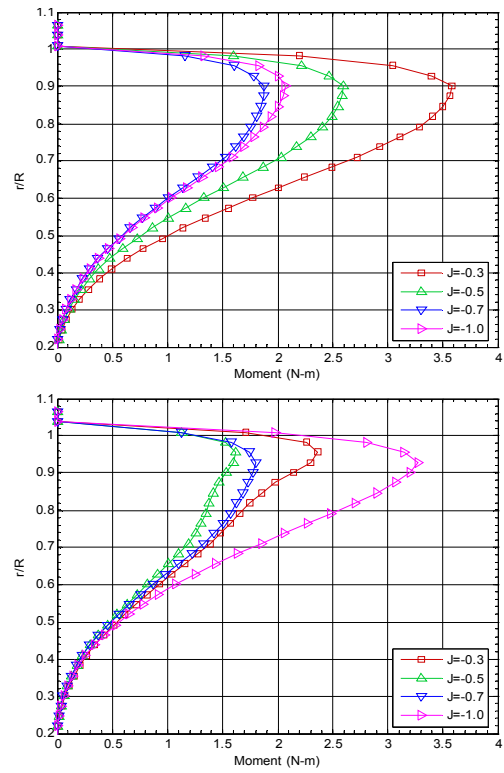


Figure 8. The mean bending moment for  $J = -0.3, -0.5, -0.7,$  and  $-1.0$  versus radius for the open configuration (top) and the ducted configuration (bottom).

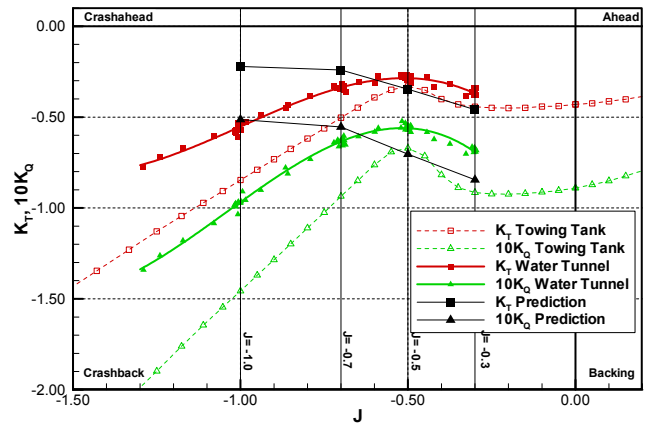


Figure 9. Mean force predictions for open 4381 predictions using PIV inflow.

Calculations at  $-0.5$  and  $-0.3$  were within reasonable agreement with the measured shaft thrust. The values at  $-0.7$  and  $-1.0$  were lower than they should be which was due to limitations in the potential flow codes for high angles of attack. To correct the mean pressure distributions, the potential flow solution was used as a starting point, and a flat plate angle of attack was superimposed on it to increase the thrust and torque loads up to those measured in the water tunnel while matching the blade element loading distribution.

After crashback operations, full scale propellers have been observed to have shifts in rake and also pitch changes at the tip. The combination of high angle of

attack and negative camber results in a crossed pressure jump across the chord of the blade. This produces a moment about the reference line of the blade, which could explain the pitch changes observed full scale.

Due to the extremely high angle of attack seen by the blade, the pressures become very low, particularly near the sharp leading edge (normally the trailing edge). For simulating surface ship propellers, the effect of cavitation on the pressure distribution has been simulated by clipping the pressure at the appropriate cavitation number in the force integration and then applying these pressures to a finite element model.

The pressure loads, viscous shear stress and centrifugal loads on the propeller in the mean crashback condition were analyzed using a finite element analysis code to predict the resultant stress levels at model scale [NE-Nastran (2001)]. The finite element model was created with the true blade geometry instead of the modified edge thickness used in the panel code. A simple model using solid brick elements with 30 elements over the span, 25 along the chord and five elements through the thickness was used in all the models. The material properties and analysis conditions corresponded to the 6061 aluminum of the model and the -700 RPM of the test condition.

The maximum principle stress distribution from the FEA analysis shows that the loading on the blade not only creates a stress concentration near the root but that the high stresses continue out along the span and move closer to what is the trailing edge in ahead operations. Near the 0.8R and 75% chord position on the blade there is a stress level that is similar in magnitude to that at the root.

The same process of computing the mean crashback loads was used for the ducted 4381 as was used for the open configuration. The circumferential mean, time averaged PIV data shown in Figure 6 and Figure 7 were used as the inflow total velocity and iterative panel method analysis was used with a field point velocity program to iterate to a converged effective inflow for the analysis. The predicted mean forces shown in Figure 10 have the same shape as the experimental data, but are roughly half the magnitude. Low forces were anticipated since no tip gap loss model was being used, but the discrepancy is larger than can be readily explained and needs further study.

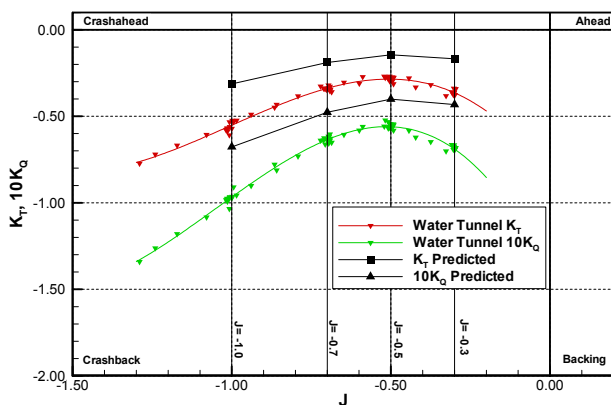


Figure 10. Mean force predictions for ducted 4381.

To correct the load to match the experiment, a flat-plate pressure distribution was added across the span. A consistent distribution of spanwise loading was maintained. The blade stress contours produced by the finite element analysis for the ducted case were found to be very similar to those of the open configuration.

## 6 EXTREME CRASHBACK ANALYSIS

The extreme blade bending moment distributions were calculated by projecting the blade geometry onto the PIV image, as shown in Figure 4, then calculating the average velocity underneath the projected outline at each radius. These velocities were then used in Equations 1 and 9 to compute the bending moment at the root for each PIV image at multiple angular projections. The velocities that caused the eight highest root bending moments were then averaged to show what conditions caused the worst case bending moments at the root. The average of the eight highest loading cases was used from all the PIV image calculations for each advanced coefficient to prevent a single outlier to skew the results.

Figure 11 shows the average axial velocities for the eight extreme bending moments. The total axial velocities moving towards the propeller for the extreme bending moment events are smaller than the time-averaged circumferential mean velocities shown in Figure 6. This result indicated that the peak bending moment occurs when the ring vortex is weaker.

Figure 12 shows the average tangential velocity of the eight cases with the most extreme bending moments. The tangential velocities are significantly higher than the time-averaged, circumferential mean values. In general the ducted tangential velocities are smaller than the open velocities, but are still significant; therefore not all of the unsteady tangential velocity was removed by the stators.

Figure 13 shows bending moment distributions that correspond to the extreme root bending moments. When compared to the bending moment distributions shown in Figure 8, the extreme distributions are at least twice the magnitude of the mean bending moments for both the open and ducted configurations.

The extreme bending moment events occur at four and five times the standard deviation of the bending moment. The root strain gauge extreme events occur at five times the standard deviation.

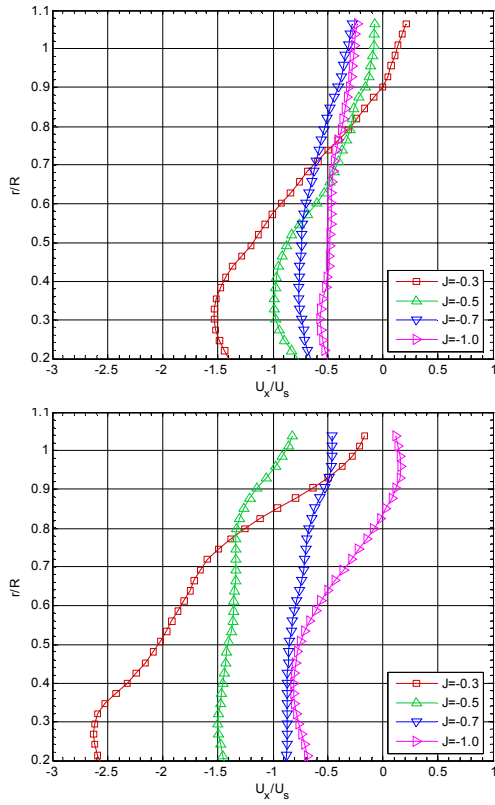


Figure 11. The average axial velocities for the extreme bending moment cases for  $J = -0.3, -0.5, -0.7$ , and  $-1.0$  versus radius for the open configuration (top) and the ducted configuration (bottom).

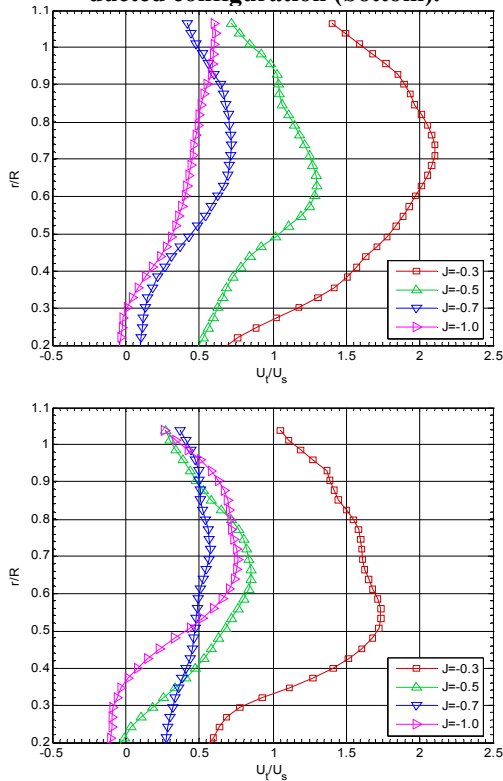


Figure 12. The average tangential velocities for the extreme bending moment cases versus radius for the open configuration (top) and the ducted configuration (bottom).

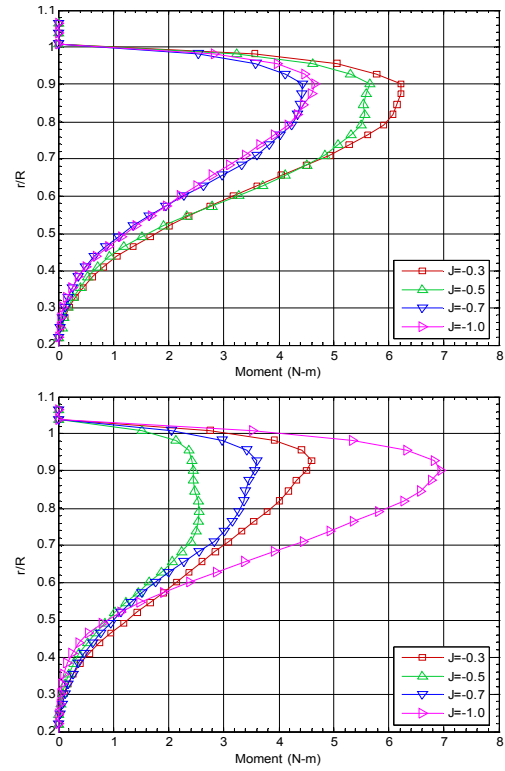


Figure 13. The maximum bending moment for eight blade projections versus radius for the open configuration (top) and the ducted configuration (bottom).

Table 1 shows the mean and extreme thrust and bending moment at the root as calculated from the PIV images for the open configuration. The bending moments varied from 1.76 to 2.27, in comparison the extreme bending moment vary from 1.70 to 2.55 times the mean bending moment when calculated from the FEA analysis. The ducted configuration results are shown in Table 2 and shows similar trends.

Table 1. Bending moment for the open configuration.

J	BM Avg. N-m	BM Ext. N-m	T Avg. (N)	T Ext. (N)	Ratio of BM	Ratio of T
-0.3	9.2	16.2	-125	-218	1.76	1.75
-0.5	6.8	15.3	-93	-206	2.24	2.22
-0.7	5.0	11.5	-69	-151	2.27	2.19
-1.0	5.4	11.6	-73	-151	2.15	2.07

Table 2. Bending moment for the ducted configuration.

J	BM Avg. N-m	BM Ext. N-m	T Avg. (N)	T Ext. (N)	Ratio of BM	Ratio of T
-0.3	5.6	11.9	-75	-159	2.12	2.12
-0.5	4.4	7.7	-60	-107	1.76	1.78
-0.7	4.8	9.8	-65	-134	2.03	2.05
-1.0	7.5	15.9	-95	-194	2.13	2.04

### Extreme to Mean Velocity Comparisons

The PIV inflow data corresponding to the eight highest bending moments were averaged to determine the worst cases shown above. The velocity distributions corresponding to the eight highest bending moments from the PIV analysis for the open propeller at  $J=-0.7$  are shown in Figure 14 and for the ducted propeller at  $J=-0.7$  in Figure 15. While the bending moments are similar for the eight inflows, the corresponding axial and tangential distributions are shown to vary significantly.

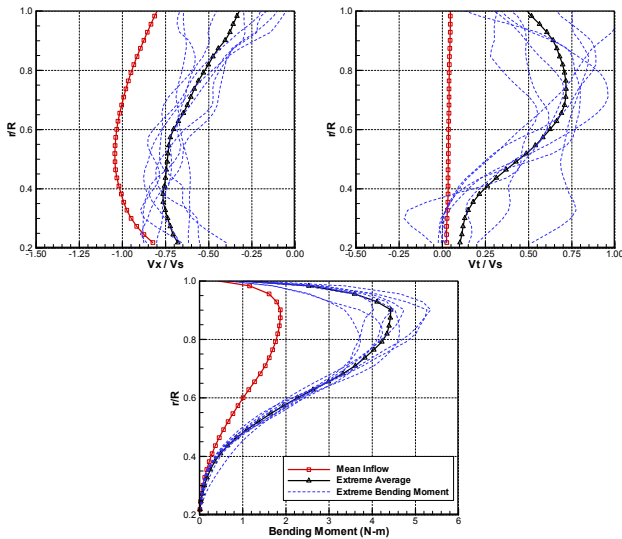


Figure 14. Mean and extreme velocities for open 4381 at  $J=-0.7$ .

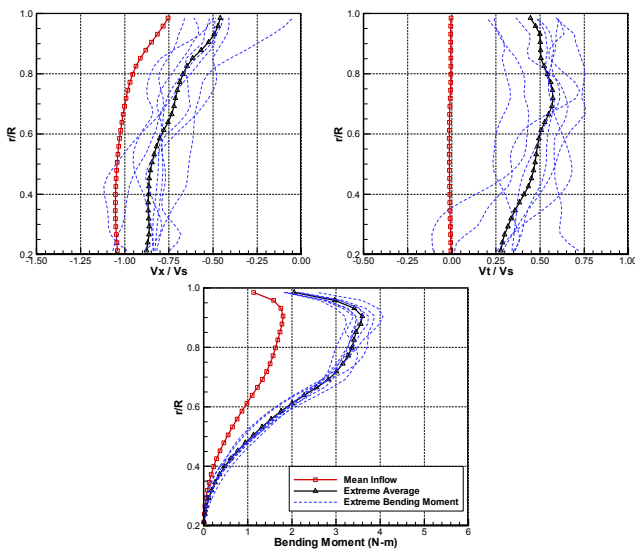


Figure 15. Mean and extreme velocities for ducted 4381 at  $J=-0.7$ .

Figure 16 shows the ratio of the axial velocities for the extreme and mean cases for both the open and ducted configuration. This ratio is less than one at radii greater than 0.6 showing that the flow is pulled into the propeller less, which would correspond to a weaker vortex ring.

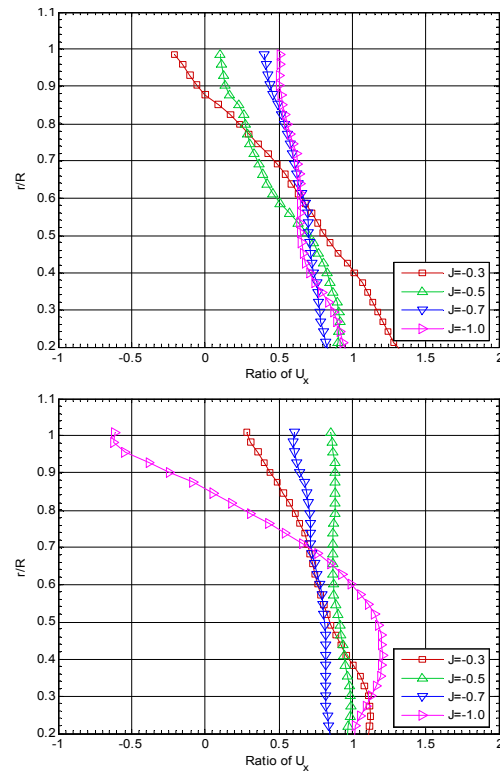
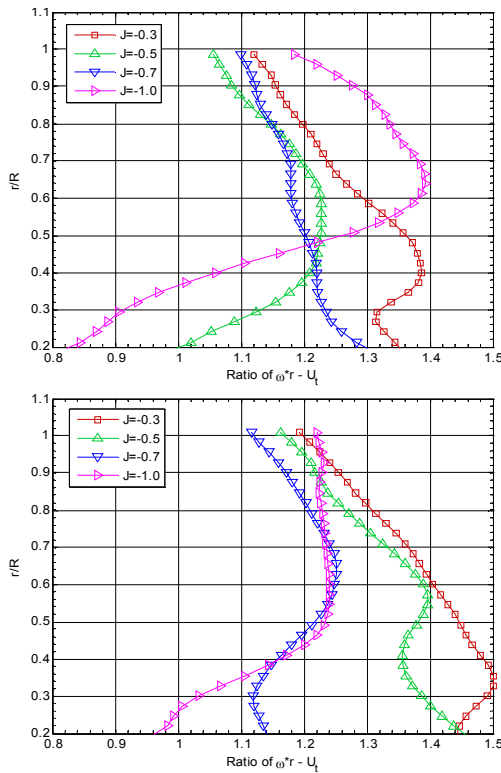


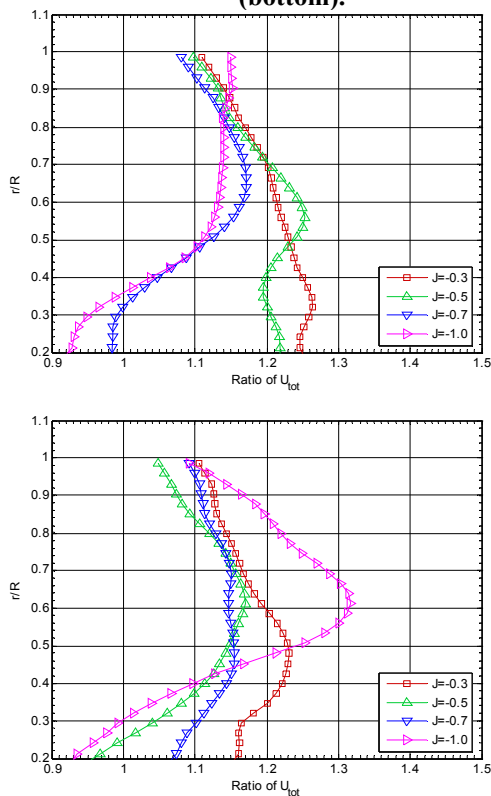
Figure 16. The ratio of the extreme load axial velocity to the mean axial velocity for the open configuration (top) and the ducted configuration (bottom).

Figure 17 shows the ratio between the total tangential velocity, including the rotational component for the extreme bending moment cases and the circumferential mean velocities. This ratio is greater than 1.0 for all radii greater than 0.4, which acts to increase the total velocity and increase the blade section angle of attack.

The other factor that largely influences root bending moment is the total velocity. Figure 18 shows the ratio of the total velocity for the extreme bending moment cases and the mean. For all radii greater than 0.4 the total velocity is greater in the extreme cases. The extreme events happen when the axial velocity is low and the tangential velocity is high, this combines to increase the angle of attack and the total velocity at the outer radii.



**Figure 17. The ratio of the extreme load tangential velocity to the mean tangential velocity for the open configuration (top) and the ducted configuration (bottom).**



**Figure 18. Ratio of the extreme total velocity to the mean total velocity.**

### Extreme Event Load Analysis

In order to develop hydrodynamic loads for a finite element analysis, the combination of angle of attack and total velocity change was used to determine a flat plate loading distribution that was super-imposed on the mean crashback load developed previously. For the extreme load analysis, a three-dimensional correction to the lift-slope is used when applying the extra angle of attack loading on the geometry. The correction is set such that the extra thrust generated results in the same extreme to mean thrust ratio as was determined by the PIV analysis. The same correction is used across the entire span, so the additional lift distribution shape is preserved, but its magnitude is scaled to produce the correct extreme-to-mean thrust ratio.

The resulting pressure distributions were used for finite element analysis for the open and ducted configurations at the four advance coefficients. The resulting distributions of maximum principle stress on the normal operation suction side are shown in the following figures. These are the same trends but with higher magnitude as was seen with the mean crashback loads analysis. There tends to be a region of high stress that extends from the root to around the 0.8 radius at the three-quarter chord position. Similar results were produced using LES calculations to provide hydrodynamic loads for finite element analysis for the same open propeller by [Chang (2008)].

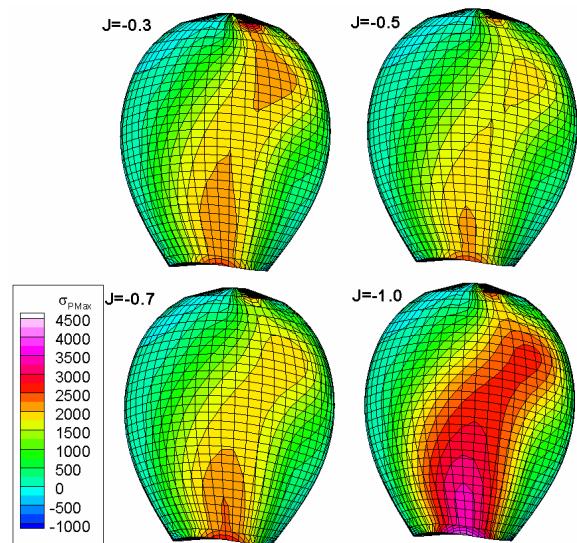


**Figure 19. Extreme crashback maximum principle stress (psi) for open 4381 at J=-0.3, -0.5, -0.7, and -1.0.**

The results from the finite element analysis for maximum principle stress are summarized in Table 3. The stress values for this propeller during steady crashback are two to three times higher than during the steady ahead condition at the same RPM. During the extreme unsteady events, the stresses can be four to six times larger than the steady ahead condition.

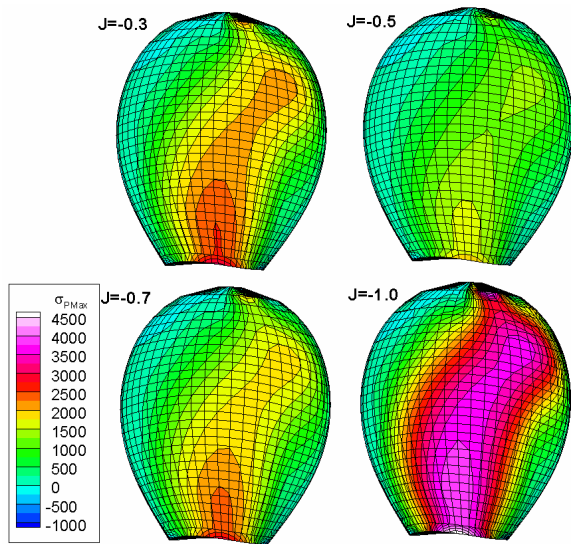


**Figure 20. Extreme crashback maximum principle stress (psi) results for ducted 4381 at J=-0.3, -0.5, -0.7 and -1.0.**

The trends for the stresses in the ducted 4381 case shown in Table 3 are very similar to those for the open propeller. The duct and struts were expected to decrease the extreme loading condition relative to the open configuration, but that was not found to be the case. It is not clear if this should be considered a representative result since, unlike typical ducted rotors, this propeller was designed to not carry any load at the tip, has short chord lengths at the tip and is operating in a neutral duct. Longer chords and more design loading near the tip for a typical ducted rotor would probably increase the tip loads during crashback. Still, this was a useful experiment to study how the duct and stators influence the crashback velocities into the rotor.

**Table 3. Maximum principle stress at 0.3R at 700 RPM.**

	Adv. Coeff. (J)	Open Mean Stress (MPa)	Open Extreme Stress (MPa)	Ducted Mean Stress (MPa)	Ducted Extreme Stress at (MPa)
Ahead	0.89	4.07	4.07	4.07	4.07
Crashback	-0.30	8.84	14.93	8.37	17.37
Crashback	-0.50	6.73	14.06	6.58	11.00
Crashback	-0.70	7.58	15.61	8.20	16.01
Crashback	-1.00	11.63	23.03	12.55	27.30

The data in Table 4 compares the maximum principle stress at the root of the propeller to the stress in the region of locally higher stress near the tip. The value near the tip tends to be lower than that at the root, but they are nearly equal at advance coefficients approaching zero. The extreme stresses near the 0.80R for the ducted rotor were proportionally similar to those for the open rotor.

**Table 4. Maximum principle stress for open 4381 during crashback.**

	J	Extreme Stress at 0.3R, 0.5c (MPa)	Extreme Stress on outer blade (MPa)	Extreme Stress Location
Crashback	-0.30	14.93	14.82	0.83R 0.75c
Crashback	-0.50	14.06	12.75	0.80R 0.75c
Crashback	-0.70	15.61	13.31	0.81R 0.75c
Crashback	-1.00	23.03	17.89	0.79R 0.75c

### 7 STRAIN COMPARISON TO EXPERIMENTS

The strain gage measurements at 0.35R acquired data at 2000 Hz. The PIV data was sampled at 35 Hz, which corresponds to the propeller rotating 120 degrees between each image. The ratio of the extreme to mean strain data and FEA analysis predictions for the open and ducted configurations are shown in Figure 21. The extreme strain gage data from the rough-order-of-magnitude (ROM) procedure are below the measurements at all advance coefficients.

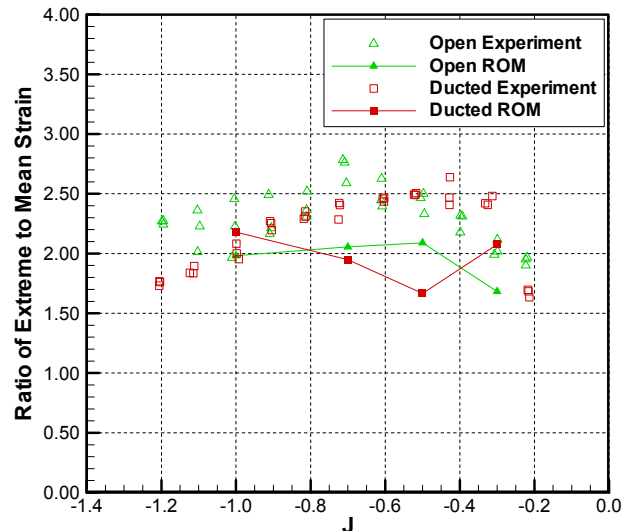


**Figure 21. Comparison of extreme to mean root strain ratio (2000Hz) to predictions.**

The 2000Hz crashback strains measured in the experiments are compared to the finite element analysis results from the ROM analysis procedure in Figure 22 for the open propeller, and in Figure 23 for the ducted unit. The mean strain values are very similar, but the extreme events are not captured as well.

The PIV images were sampled at 35 Hz whereas the strain measurements were sampled at 2000 Hz. The slower sampling rate of the PIV images could cause some of the extreme events to not be captured if they happened

between samples. When the strain measurements are resampled at 35 Hz, as shown in Figure 24, the mean values do not change significantly, but the maximum strain are lower and the ratio agrees better with the results found in this analysis. The ratio of the maximum to the mean strain is lower from the analysis of the 35Hz PIV data than for the 2000 Hz strain gauge sample rate for both the open and ducted configurations. The trend that the predicted ratio is higher than experiment could be due to a lack of a stall model in the predictions, which would reduce the extreme loads to result in a better agreement of the ratios.

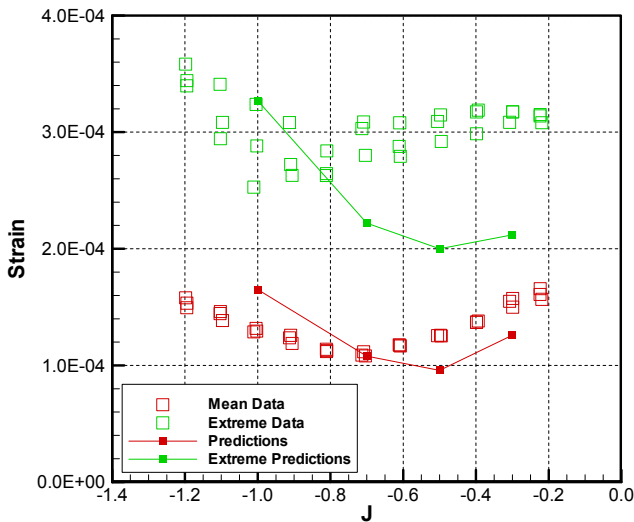


Figure 22. Strain gauge data compared predictions for open 4381.

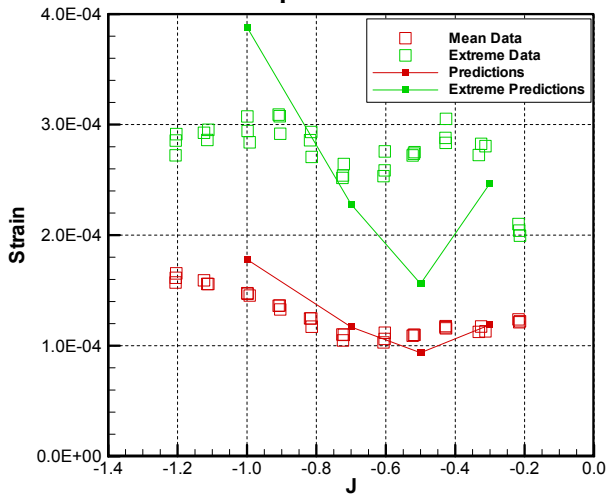


Figure 23. Strain gauge data compared to predictions for ducted 4381.

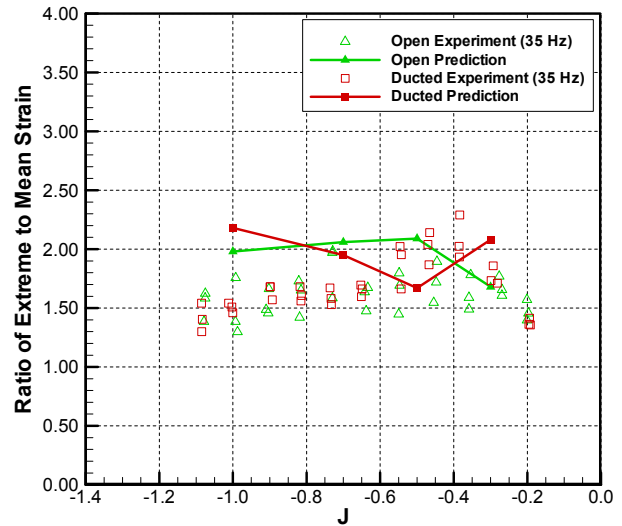


Figure 24. Comparison of extreme to mean root strain ratio (35Hz) to predictions.

In order to obtain a bending moment to strain correlation, a point load was applied to the physical model. For the range of strain seen in this experiment, the correlation between bending moment and strain was linear. The chord-wise location of the point load did not significantly change the strain. The resulting mean bending moment at the 0.35R is compared to that obtained from the PIV analysis process in Figure 25. The results are good for the ducted case, but deviate for the open geometry at the higher advance coefficients. This result is surprising since there would have been less flow separation at those conditions, which should have resulted in better agreement.

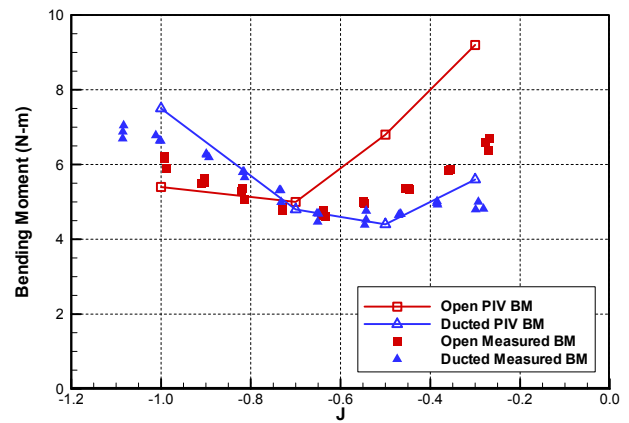
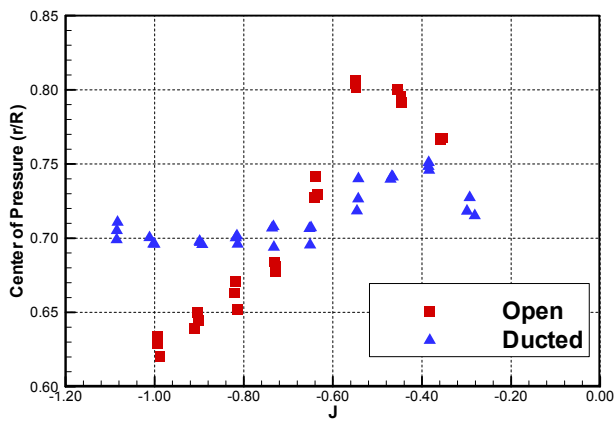


Figure 25. Average bending moment using PIV analysis compared to experimental result.

The radius of the average center of pressure can be calculated using the root bending moment and the mean thrust and torque data determined from the shaft dynamometer. The resulting radii of the center of pressure are shown in Figure 26.



**Figure 26. Radius of the average center of pressure calculated from bending moment.**

The radius of the average center of pressure varies from 0.6R to 0.8R for the open propeller, but varies much less for the ducted propeller case. This range of radii is similar to the center of pressure typically seen during ahead operation. At the lower advance coefficients (near -1.0), the open propeller will be experiencing high angles of attack near the tip, possibly resulting in stall, which would shift the center of pressure to a lower radius.

## 8 CONCLUSIONS

Based on the analysis of 4381 in the open and ducted configurations:

- The ROM structural analysis procedure produce good agreement with experimental data for the mean crashback root strain.
- The ROM structural analysis procedure for the extreme events based on the 35Hz PIV data analysis fails to capture the same extreme stain events as were measured with the 2000Hz strain experiment. It agrees well with a 35Hz strain sampling rate, indicating higher frequency PIV data is needed.
- Strain gauge data indicates that for the open and ducted 4381 propeller, the extreme strain events at the root are similar in magnitude over an advance coefficient range of -0.3 to -1.2.
- Using only the ratio in maximum to mean strain to predict unsteadiness can be misleading in selecting a worst case structural loading for assessing yield. The condition of maximum stress is more important than maximum unsteadiness.
- The stress values in the tip region for this unskewed propeller are similar between the root and tip, particularly in the advance coefficient range of -0.7 to -0.3. This result is not expected to be the case for skewed open propellers or ducted blades with finite loading and a larger chord near the tip.
- The most important crashback conditions to analyze should be those where the propeller will

be spending more time. As the ship is slowing, the propeller will spend the longest period in the advance coefficient range of -0.7 to 0.0, as was shown in Figure 1.

- Potential flow codes have the potential to provide a good first estimate at the mean crashback loading in the advance coefficient range of 0 to -0.5. At lower advance coefficients, excessive stall results in poor predictions.
- Tangential velocity significantly contributes to the extreme loading events experienced by the propellers, so previous analysis that did not include the swirl may underestimate the load.

It is proposed to use the PIV total velocity data from this propeller to analyze the performance of an open skewed propeller under the same thrust loading coefficient. It is hypothesized that to first order, the PIV data should be similar for equivalent thrust loadings. The location of blade stress concentrations are expected to be different for a skewed propeller due to the higher spindle-axis torque generated by the angle of attack loading on a skewed tip.

## REFERENCES

- Chang, P. (2008) 'Propeller Forces and Structural Response due to Crashback' 27<sup>th</sup> Symposium on Naval Hydrodynamics, Seoul, South Korea.
- Hecker, R. and K. Remmers (1971) 'Four Quadrant Open -Water Performance of Propellers 3710, 4024, 4086, 4381, 4383, 4384, and 4426', David W. Taylor Naval Research and Development Center Ship Performance Department Test and Evaluation Report, 417-H-01.
- Jessup, S.D. et al., (2004) 'Propeller Performance at Extreme Off Design Conditions,' 25<sup>th</sup> Symposium on Naval Hydrodynamics, St. John's, Newfoundland and Labrador, CANADA.
- Jessup, S. D., D. Fry and M. Donnelly, (2006) 'Unsteady Propeller Performance in Crashback Conditions With and Without a Duct' 26<sup>th</sup> Symposium on Naval Hydrodynamics, Rome, Italy.
- Kerwin, J.E. and C. S. Lee, (1978) 'Prediction of Steady and Unsteady Marine Propeller Performance by Numerical Lifting Surface Theory,' SNAME Transactions, Vol 86.
- NE/Nastran User's Manual, Version 8*, (2001) Noran Engineering, Inc.
- Swithenbank, S., Jessup, S, and Etebari, A.,(2008), 'Measurement of Crashback Loads on a Blade of Propeller 4381 in an Open and Ducted Configuration in the 36-inch Water Tunnel', NSWCCD-50-TR-2008/061.
- Vysohli, M. and K. Mahesh, (2006) 'Large Eddy Simulation of Crashback in Marine Propellers' 26<sup>th</sup> Symposium on Naval Hydrodynamics, Rome, Italy.